Bol. Soc. Paran. Mat.
©SPM – E-ISSN-2175-1188
SPM: www.spm.uem.br/bspm

(3s.) **v. 2026 (44) 17** : 1–14.
ISSN-0037-8712
doi:10.5269/bspm.82379

Analysis of Micro-Polar Fluid Flow Past a Porous Sphere using an Artificial Neural Network Approach

Aparna Podila, Kuruva Krishna Murthy, D. Sarath Chandra, M. Pavan Kumar Reddy and Atul Kaushik

ABSTRACT: The study examines the continuous flow of a micro-polar fluid through a porous sphere that is saturated with a viscous fluid, using an Artificial Neural Network (ANN) approach to determine the optimal conditions.The stream function describes the velocity field both inside and outside the sphere.The flow is regulated by non-linear partial differential equations (PDE's) in relation to the stream function, which are subjected to the corresponding boundary conditions. A novel approach to estimate solutions the Navier-Stokes equations has been developed based on artificial neural networks. We assess the scheme performance and result correctness by comparing it with established analytical methods and solutions in the literature. Tables and graphics present numerical results from analytical and ANN solutions for a wide range of physical parameter values. The results effectiveness improves when the number of neurons and the number of data points in the neural network increase. Furthermore, in contrast to the analytical approach, the existing ANN model applies to more complex mathematical frameworks as it diminishes the time and computational resources necessary for problem solving.

Keywords: Micro polar fluid, permeable sphere, ANN, r-squared.

Contents

Nomenclature

$\bar{v}$	: Velocity $[ms^{-1}]$
p	: Pressure $[pa]$
μ, k	: Viscosity coefficient $[Pa.s]$
$\bar{v}$	: Microrotation vector $[T^{-1}]$
ζ	: Stream function $[m^2 s^{-1}]$
α, β, γ	: Gyro viscosity coefficients $[Pa.S]$
a	: Radius of the sphere$[m]$
$\mathbb{C}$	: Micro rotation component $[s^{-1}]$
k^*	: Coefficient of permeability $[m^2]$
Da	: Porosity parameter (Non dimensional)

2020 *Mathematics Subject Classification:* 76A05, 76D03, 35Q30.
Submitted March 04, 2026. Published June 19, 2026.

1. Introduction

Numerous scholars have been drawn to the traditional problem of a sphere rotating steadily because it is interesting both theoretically and experimentally, and has industrial implications. The steady rotation of objects in viscous fluids is a basic problem in low–Reynolds-number hydrodynamics. It has useful uses in suspension mechanics, rheology, and fluid motion at very small scales. The first study in this area was Jeffery's [1] mathematical analysis of Stokes flow caused by a spherical rotating steadily in a viscous fluid. In his groundbreaking research, G. B. Jeffery conducted one of the first analytical analyses of the rotation of a solid of revolution in a Newtonian viscous fluid under creeping flow conditions. Ashmawy [2] formulated the problem within the Stokes flow regime, where internal effects are minimal. This simplification enables the derivation of accurate analytical expressions for the velocity field and hydrodynamic torque. His research is especially relevant in situations involving small fluid flows and biomedical applications, where slip effects can be significant due to surface roughness or rarefaction.The flow induced by a slowly rotating permeable sphere in a couple-stress fluid has been investigated by Aparna et al. [3]. According to their findings, the likelihood of fluid particles being moved away from the revolving sphere increases with larger couple stress effects, which are associated with smaller ranges for the couple stress parameter.In order to address the effects of confinement on rotational flow, Srinivasacharya and Krishna Prasad [4] examined the steady rotating motion of a composite sphere, which consists of a solid core encircled by a permeable sphere shell placed at the centre of a spherical cavity. They utilised Brinkman's model to characterise the flow inside the porous shell and applied the Stokes formulae for the adjacent viscous fluid, facilitating an analytical assessment of the hydrodynamic torque exerted on the composite particle.Aparna et al. [5] investigated the uniform flow of a viscous fluid through a porous sphere soaked with micropolar fluid. The gradual movement of micro-polar fluid around a porous sphere was examined by Srinivasacharya and Rajyalakshmi [6]. Aparna and Ramana Murthy [7] examined the flow of an incompressible micropolar fluid around a permeable sphere, addressing both interior and exterior flow areas and articulating the solution through a stream function formulation. The study conducted by Nagaraju et al. [8] examined the unstable rotary vibrations of a vertical cylinder in a Jeffery fluid with ion slip currents and a porous medium. In recent years, ANN methods have become popular as useful approaches for addressing differential equations arising in engineering applications, alongside many other machine learning methodologies. For solving differential equations, a variety of neural network methods are available, including FFNNs and Hopfield neural networks. The multilayer perceptron (MLP) is the specific sort of FFNN that is used the most frequently [9]. Analysing Magnetohydrodynamics computationally, ANN-based Jeffery-Hamel flow for couple stress fluids in stretching /shrinking channels by Atul Kaushik and Ramana Murthy [10]. One of the most important tools among them is the feed-forward neural network, which is notable for its functional flexibility, strong approximation capability, and accessibility under a diverse set of training strategies [11]. Weighted connections, concealed in one or more layers, are used by ANNs to compute facts. Each neuron in the exposed layer is connected to every neuron in the covered layer. The processing results are obtained at the output layer. Targeted training processes, extended in accordance with the principles of learning, are used to achieve learning in ANNs. A thorough overview of neural networks and a brief summary of several neural network methods for solving ODE's and PDEs were given by Yadav et al. [12] in a book. A book by Chakraverty and Mall [13] presents newly created artificial neural network models designed to address various sorts of differential equations. To solve the nonlinear ordinary differential equations, Meade [14] employed feed-forward neural networks. Neural networks provide a few benefits over more conventional approaches when it comes to solving differential equations. It is possible to view ANN as a viable substitute for analytical and numerical methods that do not necessitate solving of difficult mathematical problems. It is an effective method for solving complex engineering problems across many practical contexts and can save significant time and money. Numerous researchers have studied boundary layer flows. For example, Shahri and Nezhad [15], Ziaei-Rad et al. [16], Reddy [17], and Elayarani [18] utilized artificial neural networks (ANN) to process numerical values generated from computational methods, allowing them to calculate the skin friction factor, Nusselt number, and Sherwood number. Additionally, Nouha et al. [19] examined a Relativistic Polytropes approach using ANN. They combined the ANN-based method with the Taylor series method to numerically and computationally solve the Tolman-Oppenheimer-Volkoff equations.

Mutuk [20] examined the use of FFNN to solve the Blasius equation and provided a thorough comparison with previous studies. The study of complicated fluid flows has been greatly improved by recent developments in artificial intelligence (AI) and hybrid computational frameworks, especially in non-Newtonian and medicinal applications. To illustrate how AI frameworks can be used to investigate hemorheological properties and forecast fluid behavior in biomedical systems, Mohib Hussain et. al [21], suggested a ternary nanofluid flow analysis of blood based on artificial intelligence. A novel framework for enhanced hemorheological applications. Mohib Hussain [22] proposes a computational framework for hemodynamics simulation that integrates computational CFD, ML and AI to analyze couple-stressed hybrid nano-integrated blood flow across parallel plates subjected to peripheral squeezing. The flow of a viscous fluid across a permeable sphere was examined using an Artificial Neural Network technique by Aparna et al. [23]. They conduct a numerical investigation of how the permeability parameter influences drag and the stream function. The engineering, environmental, and biological domains are directly affected by the research of MPF fluid flow past a sphere. Applications for micropolar fluids arise when the fluid has inner microstructure and the particles may rotate independently, both of which are not possible with traditional Newtonian models. Because it more accurately describes flow behavior by taking pair stresses and microrotation effects into consideration, micropolar fluid theory is especially helpful in heat and mass transfer problems, such as those involving nanofluids and cooling systems. Ajed Akbar et al. [24] studied a neural network design to analyze magneto-hydrodynamics and heat transfer in a two-phase model of nanofluid flow with thermal radiation. An Artificial neural network analysis of an unstable fluid flow through a horizontal oscillating flat plate with a porous slab was analysed by Pothanna et al. [27]. The mathematical calculations for both exact and ANN solutions are shown in a table and a figure for a range of physical factor values. Predicting entropy generation for nanofluid flow with artificial neural networks: a study of different training algorithms was conducted by Parikshit Sharma et al. [28].

1.1. Novelty

The innovation of the proposed ANN method resides in its capacity to estimate intricate fluid flow dynamics without dependence on conventional discretization methods or closed-form analytical solutions. ANN frame work offers a mesh less, data-driven approach that accurately correlates governing parameters with flow variables. This greatly decreases computing complexity while preserving solution accuracy. A novel aspect is the direct incorporation of physical characteristics and boundary conditions into learning process, enabling the network to capture complex nonlinear interactions characteristic of advanced fluid models, including non-Newtonian fluids. ANN adeptly acquires the fundamental physics from constrained data, facilitating dependable forecasts even in parameter domains where laboratory or computational solutions are challenging to get.

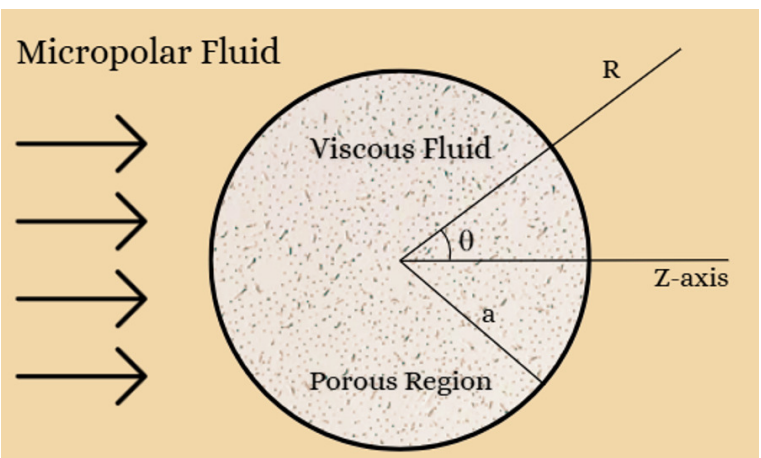

Figure 1: Geometry of the flow configuration

1.2. Aim and Research Gap

This research primarily aims to create and apply a computational framework based on ANN's for the analysis of complicated fluid flow issues driven by non linear partial differential equations. The research aims to illustrate the efficiency of ANN methodologies as reliable as well as effective substitutes for traditional analytical and numerical approaches. The paper examines a notable deficiency in existing research by analyzing the influence of couple stress parameter on velocity in relation to stream function.Prior studies have primarily focused on more straightforward models. Current ANN research frequently examines simplified configurations and lacks thorough validation across diverse physical factors. This shows how important it is to have a strong ANN-based framework for making accurate and quick flow predictions.

2. Statement of the Problem

We consider the study flow of an incompressible Micro-polar fluid past a rigid porous sphere with radius a. Within the sphere, the permeable area is completely saturated with an incompressible viscous fluid. A fixed spherical-polar coordinate frame (r, θ, φ) centered at the sphere is used to characterize the problem, with the z-axis assumed to be the direction of flow. The coordinate system's scale factors are $h_1 = 1,\ h_2 = r,\ h_3 = r\sin\theta$. The equations governing the laws of motion for a micropolar fluid in a steady-state porous media outside the sphere under the Stokesian assumption (ignoring nonlinear convective effects) are given by

$$\nabla.\bar{v}_e = 0 \tag{2.1}$$

$$0 = -\nabla p_e + k\nabla \times \bar{v}_e - (\mu + k)\nabla \times \nabla \times \bar{v}_e \tag{2.2}$$

$$0 = -2k\bar{v}_e + k\nabla \times \bar{v}_e - \gamma\nabla \times \nabla \times \bar{v}_e + (\alpha + \beta + \gamma)\nabla(\nabla \cdot \bar{v}_e) \tag{2.3}$$

The Brinkman model describes the viscous fluid movement inside the porous sphere, and the associated equations are as follows:

$$\nabla \cdot \bar{v}_i = 0 \tag{2.4}$$

$$0 = -\nabla p_i - \mu\nabla \times (\nabla \times \bar{v}_i) - \frac{\mu}{k^*}\bar{v}_i \tag{2.5}$$

By giving the axisymmetric nature of the problem, all quantities remain unchanged with respect to ϕ. To satisfy the incompressibility constraints in equations (2.1) and (2.4), the velocity is articulated by a stream function, and the micro-rotation is defined as:

$$\bar{v} = \nabla \times \left(\frac{\zeta}{h_3}\bar{e}_\varphi\right) = U_1\bar{e}_r + V_1\bar{e}_\theta \tag{2.6}$$

$$\text{and } \bar{v} = \frac{\mathbb{C}}{h_3}\bar{e}_\varphi \tag{2.7}$$

According to equation (2.6), the velocity components are defined by

$$U_1 = \frac{1}{R^2\sin\theta}\frac{\partial\zeta}{\partial\theta},\ V_1 = -\frac{1}{R\sin\theta}\frac{\partial\zeta}{\partial R}$$

Using the curl on equation (2.2) and using equations (2.6) and (2.7) we get,

$$E_0^4\left(E_0^2 - \frac{(2\mu + k)k}{\gamma(\mu + \kappa)}\right)\zeta_e = 0 \tag{2.8}$$

Now equation (2.3) becomes, by using (2.6) and (2.7)

$$\mathbb{C} = \frac{-1}{2}\left[\frac{\gamma(\mu + k)}{k^2}E_0^4\zeta + E_0^2\zeta\right] \tag{2.9}$$

$$\text{Here, } E_0^2 = \frac{\partial^2}{\partial R^2} + \left(\frac{1 - x^2}{R^2}\right)\frac{\partial^2}{\partial x^2} \tag{2.10}$$

and $x = \cos\theta$.
The dimensionless scheme is delineated as follows:

$$R = ar,\ \zeta = U_\infty a^2\psi,\ c = \frac{k}{\mu + k},\ P = \mu U_\infty a\ p,\ \mathbb{C} = U_\infty C,\ s = \frac{ka^2}{\gamma},\ E^2 = E_0^2 a^2 \text{ and } Da = k^* a^2 \tag{2.11}$$

Here uppercase letters on the left-hand side represent dimensional values, whereas the right-hand side comprises the associated non-dimensional variables expressed in lowercase italics.
After eliminating C, the equation for the internal flow's non-dimensional stream function is as follows:

$$E^2(E^2 - \lambda_1^2)\zeta_i = 0 \tag{2.12}$$

Where $\lambda_1^2 = \frac{1}{Da}$
The representation for stream function for outside flow after removing pressure using equation (2.4) and (2.5) can be obtained by

$$E^4\left[E^2 - \lambda^2\right]\zeta_e = 0 \tag{2.13}$$

Where $\lambda^2 = \frac{(2\mu+k)k}{\gamma(\mu+k)}$

2.1. Boundary Conditions

(i) On the boundary, the normal velocity remains continuous.

$$\frac{\partial\zeta_i}{\partial\theta} = \frac{\partial\zeta_e}{\partial\theta} \text{ on } r = 1$$

(ii) No-slip condition at the boundary

$$\frac{\partial\zeta_e}{\partial r} = \frac{\partial\zeta_i}{\partial r} = 0 \text{ on } r = 1$$

(iii) On a surface, the micro-rotation vector is zero.

$$C_e = 0 \text{ on } r = 1$$

(iv) Pressure continuity at the border

$$p_e = p_i$$

2.2. Analytical Examination of the Problem

The velocity equations in relation to the stream function for both the inner and outer regions are presented in equations (2.12) and (2.13).The inner and outer stream functions are provided below by the mechanism of separation of variables.

$$\zeta_e = \left(r^2 + \frac{a_1}{r} + b_1 r + c_1\sqrt{r}K_{3/2}(\lambda r)\right)G_2(x) \tag{2.14}$$

$$\zeta_i = \left[a_2 r^2 + b_2\sqrt{r}I_{3/2}(\lambda_1 r)\right]G_2(x) \tag{2.15}$$

3. ANN Approach

Artificial neural networks (ANNs) can analyze training data for patterns and correlations without human intervention. Unlike traditional models, ANNs can handle nonlinear relationships between inputs and outputs. By leveraging the function approximation capabilities of feedforward neural networks (FFNNs) to enhance solutions, the primary goal of artificial neural networks is to develop effective solutions. A neural network-like pattern is produced by the discrepancy between the numerically generated outcomes and the squared error values. Reducing loss requires either training or modifying the FFNN's bias and weights. Optimisation techniques that compute error gradients with respect to the input variables and the neural network are required. The first approach put forth by Lagaris [25] is depicted as

the product of two parts. One part concerns the neural network's parameters, and the other satisfies the peripheral conditions.

On the other hand, the boundary conditions dictate the type of initial solution that must be chosen for this. With certain boundary limitations, it is difficult to choose an appropriate initial solution. Piscopo et al. [26] proposed the first approach to depicting the network output by adding boundary constraints to the loss function as additional terms. Consider a multilayer perceptron (MLP) with three layers, featuring an input layer with, Secret layer consisting of k neurons and an output layer comprising a single neuron to approximate the solution of the PDE, as illustrated in Figure 2.

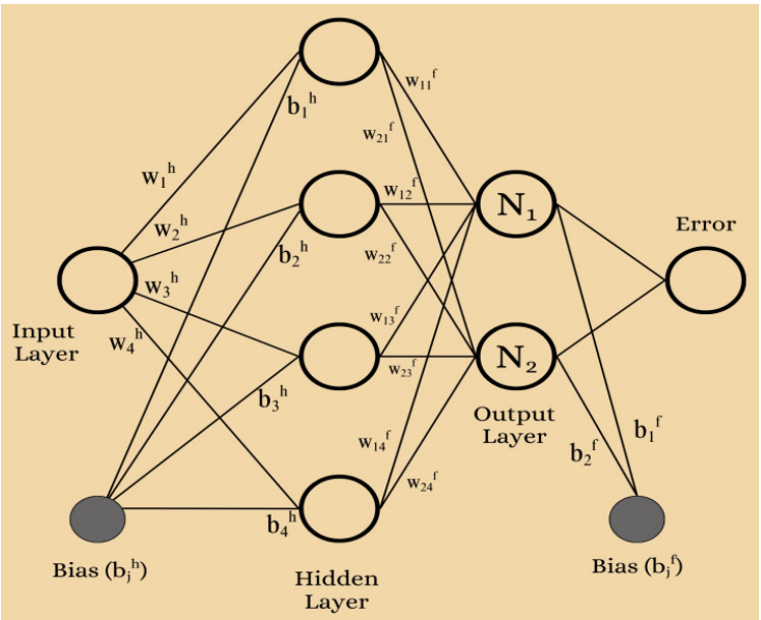

Figure 2: Neural network model

In Figure 2 we can see the detailed process of using feed-forward ANNs to solve the micro-polar MPF flow through a sphere problem. At first, we use the analytical method to establish our model equations and get a solution. With these numbers in hand, we can decide how many ANN layers to utilize for training and testing the network. Picking the optimal neuronal density until optimal regression was achieved (i.e., $R > 1$) was our primary goal here. Upon completion of this task, we train the model with varying numbers of neurons in order to make predictions and test the data. Considering that MLP has three levels, an input layer with inputs is the first having, $\bar{r} = (r_1, r_2, r_3, \ldots r_m)$, a concealed layer consisting of 'm' neurons and a production layer consisting of a single neuron to estimate the solution of the partial differential equation, as illustrated in Figure **??**. As illustrated in Figure **??**, the output for internal flow is considered as $N_1(r_i, P_1)$. The test solution for the stream function, with the adjustable parameter P_1, is indicated by the network output $N_2(r_i, P_1)$, which is represented by the formula

$$N_1(r_i, P_1) = \sum_{j=1}^{k} \bar{w}_{1j}^f \sigma \left\{ \bar{w}_j^h r_i + b_j^h \right\} + b_1^f \tag{3.1}$$

The output for external flow is considered as $N_2(r_i, P_2)$.The test solution for the stream function, with the adjustable parameter P_2, is indicated by the network output$N_2(r_i, P_2)$, which is represented by the formula

$$N_2(r_i, P_2) = \sum_{j=1}^{k} \bar{w}_{2j}^f \sigma \left\{ \bar{w}_j^h y_i + b_j^h \right\} + b_2^f \tag{3.2}$$

Here, superscript 'h' stands for the hidden layer, 'f' for the final layer, and σ for the activation function applied to each component separately. $\bar{w}_j^h$ Indicates the layer that is hidden. Weights from the entering

layer to the j^{th} hidden neuron indicate the weight between the j^{th} hid neuron and the k^{th} output neuron, whereas the bias term in the hidden by $\bar{w}^f_{kj}$. P_1 aligns with the parameters $\bar{w}^h_j$, b^h_j, $\bar{w}^f_{1j}$, b^f_1.P_2 is connected with $\bar{w}^h_j, b^h_j, \bar{w}^f_{2j}, b^f_2$.

In terms of the input vectorr_i, the network output parameters $N_1(r_i, P_1)$ and $N_2(r_i, P_2)$ have the following derivatives:

$$\frac{\partial N_1}{\partial r_i} = \frac{\partial}{\partial r_i}\sum_{j=1}^{k} \bar{w}^f_{1j}\sigma\left\{\bar{w}^h_j r_i + b^h_j\right\} + b^f_1 = \sum_{j=1}^{k} \bar{w}^h_j \bar{w}^f_{1j}\sigma'_i$$

$$\frac{\partial N_2}{\partial r_i} = \frac{\partial}{\partial r_i}\sum_{j=1}^{k} \bar{w}^f_{2j}\sigma\left\{\bar{w}^h_j r_i + b^h_j\right\} + b^f_2 = \sum_{j=1}^{k} \bar{w}^h_j \bar{w}^f_{2j}\sigma'_i$$

Where $\sigma'_j = \frac{\partial\sigma(r_i)}{\partial r_i}$

Similarly, $\frac{\partial^n N_1}{\partial r_i^n} = \sum_{j=1}^{k} \bar{w}^h_j \bar{w}^f_{1j}\sigma^{(n)}_i$ and $\frac{\partial^n N_2}{\partial r_i^n} = \sum_{j=1}^{k} \bar{w}^h_j \bar{w}^f_{2j}\sigma^{(n)}_i$

Substituting Eq. (3.1) and (3.2) in the Eqs. (2.2) and (2.5), we obtain the subsequent partial differential equations for external and internal flows are given by,

$$\left(\frac{\partial^2}{\partial r_i^2}(N_1) + \frac{1}{r_i}\frac{\partial}{\partial r_i}(N_1) + \frac{1}{r_i^2}\frac{\partial^2}{\partial\theta^2}(N_1)\right)^2 \left[\frac{\partial^2}{\partial r_i^2}(N_1) + \frac{1}{r_i}\frac{\partial}{\partial r_i}(N_1) + \frac{1}{r_i^2}\frac{\partial^2}{\partial\theta^2}(N_1) - \lambda^2 N_1\right] = 0 \quad (3.3)$$

and

$$\left(\frac{\partial^2}{\partial r_i^2}(N_2) + \frac{1}{r_i}\frac{\partial}{\partial r_i}(N_2) + \frac{1}{r_i^2}\frac{\partial^2}{\partial\theta^2}(N_2)\right) \left[\frac{\partial^2}{\partial r_i^2}(N_2) + \frac{1}{r_i}\frac{\partial}{\partial r_i}(N_2) + \frac{1}{r_i^2}\frac{\partial^2}{\partial\theta^2}(N_2) - \lambda^2 N_2\right] = 0 \quad (3.4)$$

As N_1 and N_2 are approximated solutions, so they will not exactly satisfy equations (2.12) and (2.13), which will lead to residual.

$$\left(\frac{\partial^2}{\partial r_i^2}(N_1) + \frac{1}{r_i}\frac{\partial}{\partial r_i}(N_1) + \frac{1}{r_i^2}\frac{\partial^2}{\partial\theta^2}(N_1)\right)^2 \left[\frac{\partial^2}{\partial r_i^2}(N_1) + \frac{1}{r_i}\frac{\partial}{\partial r_i}(N_1) + \frac{1}{r_i^2}\frac{\partial^2}{\partial\theta^2}(N_1) - \lambda^2 N_1\right] = R_1$$

$$\left(\frac{\partial^2}{\partial r_i^2}(N_2) + \frac{1}{r_i}\frac{\partial}{\partial r_i}(N_2) + \frac{1}{r_i^2}\frac{\partial^2}{\partial\theta^2}(N_2)\right) \left[\frac{\partial^2}{\partial r_i^2}(N_2) + \frac{1}{r_i}\frac{\partial}{\partial r_i}(N_2) + \frac{1}{r_i^2}\frac{\partial^2}{\partial\theta^2}(N_2) - \lambda^2 N_2\right] = R_2$$

Boundary conditions loss:

$$L_{bc} = \frac{1}{n}\left[(\frac{\partial\zeta_i}{\partial\theta} - \frac{\partial\zeta_e}{\partial\theta})^2 + (\frac{\partial\zeta_e}{\partial r} - \frac{\partial\zeta_i}{\partial r})^2 + C_e^2 + (p_e - p_i)^2\right]_{r=1}$$

The loss function for internal and external flows is given by

$$L_{total} = \frac{1}{n}\left[\sum R_1^2 + \sum R_2^2 + L_{bc}\right]$$

4. Advantages and Limitations of the Proposed Approach

The proposed ANN methodology effectively addresses the nonlinearities in the governing equations governing intricate fluid flow without requiring mesh generation.This mesh-free attribute markedly reduces computational cost and facilitates a seamless solution estimation throughout the entire domain. The ANN model is well-suited for parametric and sensitivity studies because, once trained, it enables fast forecasting of flow parameters for different parametric values. Nevertheless, selecting the right network design and training the parameters have a significant impact on the artificial neural network (ANN) model's performance. When tuning is not done properly, overfitting or underfitting might happen. Furthermore, ANN models are not directly physically interpretable because of their black-box character, and training can be costly in comparison to analytical or conventional numerical methods.

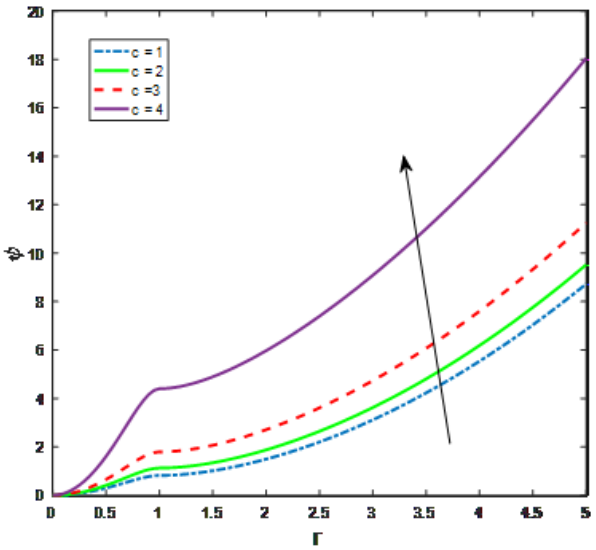

Figure 3: Stream function vs Distance for $\theta = \frac{\pi}{3}, Da = 0.04, s = 1.2$.

In Figure 3, the stream function variation is shown for a range of cross viscosity parameter $'c'$ values. The figure illustrates the fluctuation of the stream function ψ with radial distance 'r' for various values of the parameter $'c'$, while maintaining constant values for $\theta = \frac{\pi}{3}$, s = 1.2, and Da = 0.04. The stream function curves continuously shift upward as the parameter 'c' increases from 1 to 4. This suggests that higher values of c increase the domain's flow intensity. In all instances, ψ exhibits a monotonically increasing behavior with respect to r, with the rate of growth intensifying for elevated values of c. The curves stay narrow and close together around the origin, indicating a weak dependency on 'c' at small radial distances. As r grows, the divergence between the curves gets increasingly pronounced, indicating that the effect of c is more predominant in the outer boundaries of the flow field. The results indicate that an increase in c significantly elevates the stream function, suggesting improved fluid flow and momentum transfer. The ψ values are rising in line with the 'c' values. Figure 3 shows that the values of the stream function decline as 'c' goes to zero. A viscous fluid is generated as 'c' goes to zero. As a result, we note that the stream function of a viscous fluid will be smaller than that of a micro-polar fluid.

The illustration depicts the variation of the stream function ψ with respect to distance 'r' for various values of the parameter s. The value of ψ always goes up as we move farther away from the center. This means that the flow of the fluid gets stronger as we move farther away. We can see that lesser values of 's' lead to larger stream function values when we compare the shapes.

The stream function's change for various coupling stress parameter values is shown in Figure 4. The values of ψ are dropping as s increases. We obtain a viscous fluid scenario in the special case as $s \to \infty$. Because of this, we know that viscous fluids' stream functions will be smaller than micro-polar fluids.

Figure 5 illustrates the radial variation of the stream function for three different porosity parameter values (Da = 0.05,Da= 0.1, Da = 0.15) at fixed parameter values of $\theta = \frac{\pi}{3}, c = 0.5, s = 1.2$. The stream function decreases monotonically with radial distance, indicating a smooth outward flow pattern in the domain under consideration. The primary influence observed in the figure is the effect of the Deborah number, which characterizes the elastic nature of the Jeffery fluid. A lower Deborah number (Da=0.05) corresponds to high elastic effects, and the resulting stream function displays relatively higher values across the domain. As the porosity parameter values grow to 0.05 and 0.15, the stream function values significantly elevate at the same radial places. A reduced porosity parameter indicates that the fluids elastic relaxation period is more prominent relative to the flow time scale. The inner radial region is where the discrepancies between the curves are most noticeable, suggesting that elasticity is more important near the sphere's surface. The finding absolutely shows that lowering the porosity parameter increases flow

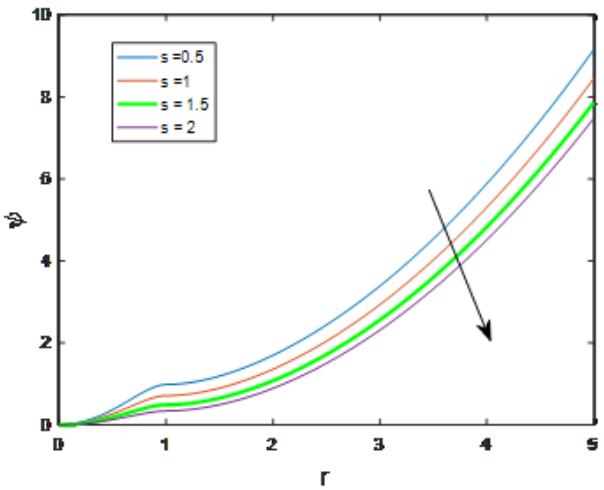

Figure 4: Stream function vs Distance for $\theta = \frac{\pi}{3}, c = 0.3, Da = 0.005$.

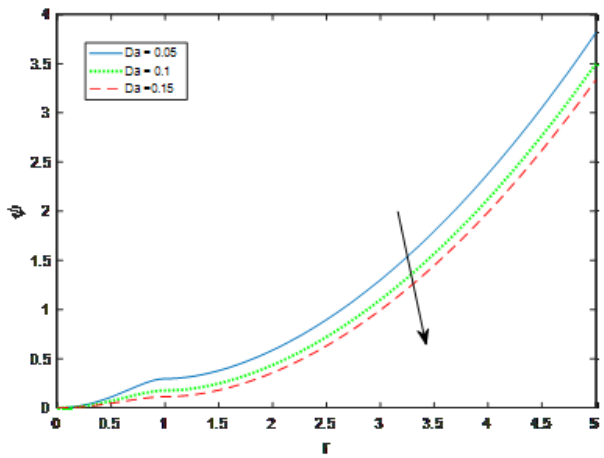

Figure 5: Stream function vs Distance for $\theta = \frac{\pi}{3}, c = 0.5, s = 1.2$.

intensity and raises stream function values. Particularly in cases involving polymeric fluids, viscoelastic suspensions, and procedures where relaxation effects impact flow behavior, fluid elasticity becomes crucial in fluid dynamics.

Figure 6 shows how the stream function varies with distance for various values of the parameter c (c = 0.8, 1.6, 2.4) for fixed value of $\theta = \frac{\pi}{3}, Da = 0.05, s = 1.2$.

The stream function directly measures the flow rate, thus how it behaves gives us a clear picture of how the fluid moves. It is clear from the illustration that the stream function grows gradually with distance for all values of 'c', suggesting that the flow gets stronger and stronger as the distance increases. The extremely close spacing of the curve near to the origin indicates that 'c' has a negligible impact in the area. The increasing impact of 'c' on the flow field is shown by the increasing separation between the curves as distance grows. The stream functions magnitude is amplified across the domain as the parameter 'c' raised. Specifically, bigger values of 'c' indicate stronger fluid flow or circulation since streamlines are more prominent. According to the governing model's physical interpretation, this behavior suggests that 'c' is a flow enhancing parameter, possibly associated with fluid micro structure effects, permeability or relaxation properties. Due to the combined effects of geometry and the regulating physical parameters,

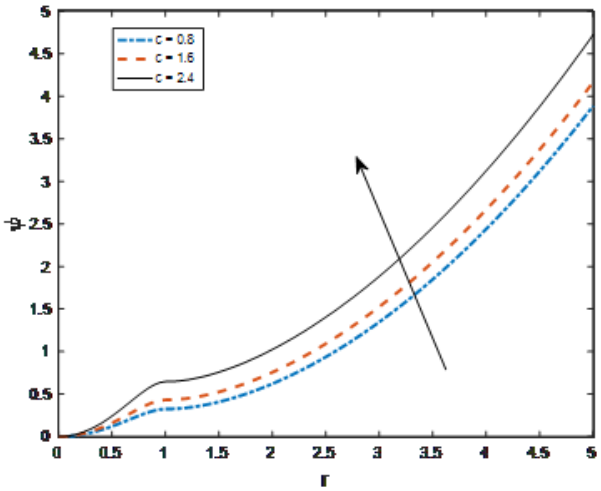

Figure 6: Stream function vs Distance for $\theta = \frac{\pi}{3}, Da = 0.05, s = 1.2$

the progressive acceleration of the flow, rather than a linear one, is suggested by the fact that ψ rises nonlinearly with distance.

The graphic illustrates that the stream function exhibits significant sensitivity to variations in 'c' at greater distances, while displaying relative insensitivity non the starting region. This tendency is physically significant and verifies that modifying C can successfully regulate the flow intensity inside the system in concern.

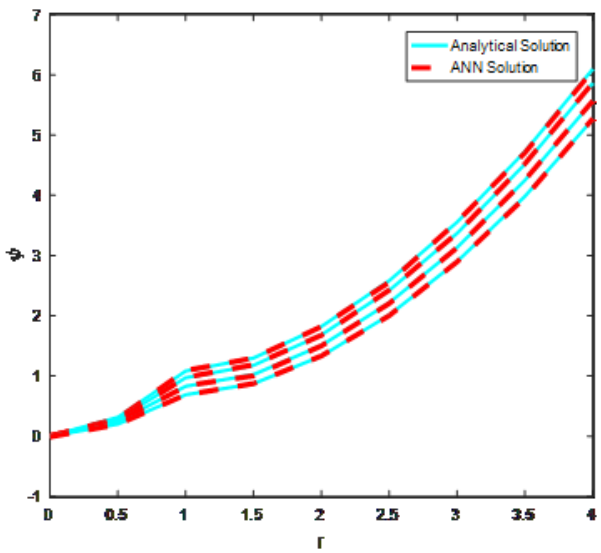

Figure 7: Comparison of Artificial Neural Networks and Analytical Methods for Streamline Variation Across Different Values of 's' for $\theta = \frac{\pi}{3}, c = 0.3, Da = 0.005$

As shown in Figure 7 for different values of 's',the analytical solution and the Artificial Neural Network (ANN) solution for the change of the stream function with 'r' at $\theta = \frac{\pi}{2}$ are compared. In order to determine how well the ANN method captures the flow properties determined by the analytical model, we will compare the two methods. The purpose of this comparison is to evaluate the accuracy and dependability of the ANN technique in terms of its capacity to capture the flow characteristics that

are predicted by the analytical model. The figure makes it abundantly clear that the ANN solutions are in perfect agreement with the analytical conclusions that correspond to them for each and every value of 's' that was taken into consideration. The neural network model's durability and accuracy in approximating the governing flow equations are demonstrated by the fact that the ANN curves nearly overlap the analytical curves across the whole radial domain, with no discernible deviations. As the radial distance r increases, the stream function exhibits a continuous rise for all values of 's', indicating that the flow intensity is growing far from the surface. Stronger fluid movement in the outer portion of the flow field is shown by the increase of ψ, which is more gradual for smaller values of r but steeper at larger values of 'r'. Increasing the permeability parameter also results in greater values of the stream function at a given radial point. As the permeability parameter is raised, the stream function also shows greater values at a specific radial position. This pattern suggests that mediums with higher permeability allow fluids to pass through more readily, resulting in larger circulation and more intense flow.

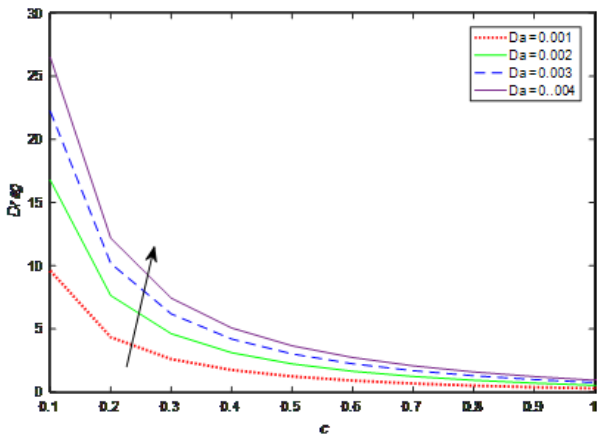

Figure 8: c versus Drag for various values of Da for $s = 5$

The Figure 8 illustrates the variation of the drag coefficient with the parameter 'c' for different values of the porosity parameter (Da). For all considerable cases, the drag coefficient decreases steadily as 'c' increases, indicating that higher values of 'c' are associated with reduced flow resistance. For fixed values of 'c', the drag coefficient is noticeably higher at lower values of porosity parameter. In particular, the curve corresponding to Da = 0.005 shows a maximum drag, while the minimum drag is observed for Da = 0.02. This trend reflects the influence the porosity.

Smaller value of 'Da' corresponds to lower porosity, which restricts fluid motion and enhance drag. As 'c' increases further, the rate of decrease become gradual and curves for different porosity parameters tend to converge, implying that the effect of porosity becomes less dominant at higher values of 'c'.

Table 1: Analytical and ANN calculations for Drag function across diverse material properties

	Analytical Solution ($Da = 0.05, \mathrm{s} = 1.2,\ \mathrm{c} = 0.3$)			ANN solution ($Da = 0.05, \mathrm{s} = 1.2,\ \mathrm{c} = 0.3$)		
r	$\theta = \frac{\pi}{3}$	$\theta = \frac{2\pi}{3}$	$\theta = \frac{4\pi}{3}$	$\theta = \frac{\pi}{3}$	$\theta = \frac{2\pi}{3}$	$\theta = \frac{4\pi}{3}$
0	0	0	0	0	0	0
0.5	0.2283775	0.228377524	0.228377524	0.2467163	0.228257523	0.2273675
1	0.6098839	0.609883961	0.609883961	0.6096839	0.609783361	0.6097739
1.5	0.7857076	0.785707625	0.785707625	0.7862893	0.785507525	0.7858166
2	1.2311049	1.231104952	1.231104952	1.2310280	1.231004852	1.2311147
2.5	1.8968317	1.896831744	1.896831744	1.8954958	1.896631544	1.8967316
3	2.7664732	2.766473269	2.766473269	2.7668995	2.766563269	2.7663532
3.5	3.8329946	3.832994642	3.832994642	3.8387786	3.832764642	3.8327646
4	5.0928784	5.092878418	5.092878418	5.0915727	5.092668316	5.0926684

Table 2: Comparison of results for Stream function: Stream function ψ for ($Da = 0.05, \theta = \frac{\pi}{5}, s = 1.2$)

	Present results			Results of Aparna et.al [7]		
r	c = 0.8	c = 1.6	c = 2.4	c = 0.8	c = 1.6	c = 2.4
0	0	0	0	0	0	0
0.5	0.16	0.93	0.2422	0.14	0.918	0.2425
1	0.3247	0.4323	0.6468	0.325	0.4322	0.6467
1.5	0.4093	0.5259	0.7583	0.4093	0.5262	0.7581
2	0.6218	0.7563	1.024	0.622	0.7553	1.024
2.5	0.9372	1.093	1.404	0.9372	1.096	1.404
3	1.347	1.527	1.844	1.342	1.528	1.848

Table 1 shows the results of Analytical and ANN calculations for the stream function for different types of materials. Table 2 compares the numerical stream-function results to the ones that Aparna et al. [7] published. The tight agreement shows that the current analysis is correct.

5. Conclusions

The findings obtained from governing equations utilizing ANN, incorporating the influence of various material characteristics, have been analyzed and represented with distinct numerical values. This study is very helpful for scientific and academics who are trying to solve problems in industry and research. Over the past several decades, there has been significant rise in interest in the study of flow characteristics within these configurations, owing to their extensive range of applications.

1. As the number of data points and hidden neurons increases, the resultant analytical solution exhibits a very excellent agreement with ANN solution.

2. Variations in porosity, couple stress parameter and cross viscosity parameter have been an impact on both internal and external flow.

3. The ANN approach provides flexible, data driven approaches that can deal with complex non-linearities and flow dynamics.

4. ANN based solvers are employed to address more complex flow systems, such as Non – Newtonian fluids.

5. The ANN framework effectively captured the impact of important physical parameters on the flow characteristics.

6. The ANN model correctly forecasts the stream function characteristics and it agrees closely with analytical results for extensive number of governing equatins.

7. The ANN model effectively captured the nonlinear characteristics of the velocity field and demonstrated strong agreement with the analytical solutions across a wide range of physical parameters.

8. The outcomes confirm that the ANN method is a precise and effective alternative to traditional numerical techniques for solving complex non-Newtonian fluid flow problems. It minimizes computational effort while maintaining high prediction accuracy, making it especially suitable for parametric studies and real-time applications.

Future research may extend the present work to unsteady flows, heat and mass transfer analysis, and different geometrical configurations. Additionally, hybrid models combining ANN with physics-informed neural networks (PINNs) or experimental validation could further enhance prediction reliability and broaden practical applications.

References

1. Jeffery, G. B., *Steady rotation of a solid of revolution in a viscous fluid*, Proc. Lond. Math. Soc. 14, 327–338, (1915).
2. Ashmawy, E. A., *Slip at the surface of a general axi-symmetric body rotating in a viscous fluid*, Arch. Mech. 63(4), 341–360, (2011).
3. Aparna, P., Ramana Murthy, J. V. and Nagaraju, G., *Couple on a rotating permeable sphere in a couple stress fluid*, Ain Shams Eng. J., (2016).
4. Srinivasacharya, D. and Krishna Prasad, M., *Steady rotation of a composite sphere in a concentric spherical cavity*, Acta Mech. Sin. 28(3), 653–658, (2012).
5. Aparna, P., Padmaja, P., Pothanna, N. and Ramana Murthy, J. V., *Uniform flow of viscous fluid past a porous sphere saturated with micropolar fluid*, Biointerface Res. Appl. Chem. 13(1), 69, (2023).
6. Srinivasacharya, D. and Rajyalakshmi, I., *Creeping flow of micropolar fluid past a porous sphere*, Appl. Math. Comput. 153(3), 843–854, (2004).
7. Aparna, P. and Ramana Murthy, J. V., *Uniform flow of an incompressible micropolar fluid past a permeable sphere*, Int. e-J. Eng. Math.: Theory Appl. 8, 1–10, (2010).
8. Nagaraju, G. and Aparna, P., *Unsteady rotatory oscillations of a vertical cylinder in jeffery fluid with ion slip currents and porous medium*, Int. J. Eng. Technol. 7(4), 6592–6596, (2018).
9. Pham, D. T. and Liu, X., *Neural Networks for Identification, Prediction and Control*, Springer, London, (1995).
10. Kaushik, A. and Ramana Murthy, J. V., *Computational analysis of magnetohydrodynamic jeffery–hamel flow for couple stress fluids in stretching/shrinking channels via artificial neural network*, Int. J. Numer. Methods Eng. 126, e70174, (2025).
11. Lee, H. and Kang, I. S., *Neural algorithm for solving differential equations*, J. Comput. Phys. 91, 110–131, (1990).
12. Yadav, N., Yadav, A. and Kumar, M., *An Introduction to Neural Network Methods for Differential Equations*, Springer, Dordrecht, (2015).
13. Chakraverty, S. and Mall, S., *Artificial Neural Networks for Engineers and Scientists: Solving Ordinary Differential Equations*, CRC Press, Boca Raton, FL, (2017).
14. Meade, A. J. and Fernandez, A. A., *Solution of nonlinear ordinary differential equations by feedforward neural networks*, Math. Comput. Modell. 20, 19–44, (1994).
15. Shahri, M. F. and Nezhad, A. H., *Estimation of the flow and heat transfer in mhd flow of a power law fluid over a porous plate using artificial neural networks*, Middle East J. Sci. Res. 22, 1422–1429, (2014).
16. Ziaei-Rad, M., Saeedan, M. and Afshari, E., *Simulation and prediction of mhd dissipative nanofluid flow on a permeable stretching surface using artificial neural network*, Appl. Therm. Eng. 99, 373–382, (2016).
17. Reddy, P. B. A. and Das, R., *Estimation of mhd boundary layer slip flow over a permeable stretching cylinder in the presence of chemical reaction through numerical and artificial neural network modeling*, Eng. Sci. Technol., Int. J. 19, 1108–1116, (2016).
18. Elayarani, M. and Shanmugapriya, M., *Artificial neural network modeling of mhd stagnation point flow and heat transfer towards a porous stretching sheet*, AIP Conf. Proc. 2161, 020043, (2019).
19. Nouha, M. I., Abdel-Salam, E. A.-B. and Azzam, Y. A., *Artificial neural network approach for relativistic polytropes*, Sci. Afr. 20, e01696, (2023).
20. Mutuk, H., *A neural network study of blasius equation*, Neural Process. Lett. 51, 2179–2194, (2020).

21. Hussain, M., Waqas, H., Ali, B. and Shah, N. A., *Predicting radiative flow and heat transfer in ternary nanofluids: a hybrid graph neural network and finite difference framework with cattaneo–christov theory*, Thermal Sci. Eng. Prog. 66, 103982, (2025).

22. Hussain, M., Lin, D., Waqas, H. and Al-Mdallal, Q. M., *An artificial intelligence and machine learning-driven cfd simulation for optimizing thermal performance of blood-integrated ternary nanofluid*, (2025).

23. Aparna, P., Ganesh Kumar, V., Padmaja, P. and Niranjan, H., *Viscous fluid flow past a permeable sphere–ann approach*, Int. J. Thermofluids 30, 101475, (2025).

24. Akbar, A., Ullah, H., Raja, M. A. Z., Nisar, K. S., Islam, S. and Shoaib, M., *A design of neural networks to study mhd and heat transfer in two phase model of nanofluid flow in the presence of thermal radiation*, 1–24, (2022).

25. Lagaris, I. E., Likas, A. and Fotiadis, D. I., *Artificial neural networks for solving ordinary and partial differential equations*, IEEE Trans. Neural Networks 9, 987–1000, (1998).

26. Piscopo, M. L., Spannowsky, M. and Waite, P., *Solving differential equations with neural networks: applications to the calculation of cosmological phase transitions*, Phys. Rev. D 100, 016002, (2019).

27. Nalimela, P., Thirmal, C., Kumar, V. G. and Reddy, G. J., *Artificial neural networks analysis of an unsteady fluid flow through a horizontal oscillating flat plate in a porous slab*, Phys. Fluids 37, 023140 (2025).

28. Sharma, P., Sharma, B. K., Sharma, M., Almohse, B. and Urbanowicz, K., *Entropy generation prediction for nanofluid flow using artificial neural networks: a comparative study of training algorithms*, J. Therm. Anal. Calorim. 150, 14477–14500, (2025).

Aparna Podila,
Department of Mathematics,
VNR Vignana Jyothi Institute of Engineering and Technology,
Hyderabad-500118, Telangana State, India.
E-mail address: aparnapodila@gmail.com

and

Kuruva Krishna Murthy,
Department of Mechanical Engineering,
VNR Vignana Jyothi Institute of Engineering and Technology,
Hyderabad-500118, Telangana State, India.
E-mail address: murthy2164@gmail.com

and

D. Sarath Chandra,
Department of Mechanical Engineering,
VNR Vignana Jyothi Institute of Engineering and Technology,
Hyderabad-500118, Telangana State, India.
E-mail address: sarathchandra_d@vnrvjiet.in

and

M. Pavan Kumar Reddy,
Department of Mathematics,
VNR Vignana Jyothi Institute of Engineering and Technology,
Hyderabad-500118, Telangana State, India.
E-mail address: mprnitw@gmail.com

and

Atul Kaushik,
Department of Mathematics,
National Institute of Technology,
Warangal, India.
E-mail address: ak22mar1r06@student.nitw.ac.in